

Chapter 6

**Synthesis and Characterization of Cu-Fe₂O₃ and CuNi
Nanoparticles and their Catalytic Activity for the Reduction
of Nitroaromatics Compounds**

Outline

Toxicity of nitro aromatic compounds is well known in the world of chemistry, although they are used in huge amounts as pesticides, pharmaceutical, explosives, dyes and in chemical industries [1]. The aromatic nitro compounds such as nitrobenzene, nitrotoluenes, nitrophenol in natural water and effluents has attracted considerable attention for environmental control due to their wide range of toxic effects on human, animals and plants. Among them 4-nitrophenol (4-NP) is listed as major pollutant by USA EPA due to its chemical, biological stability and difficult to be removed by natural degradation [2–4]. Several processes have introduced to reduce the harmful effect of 4-NP such as adsorption [5], microbial degradation [6], photo catalytic degradation [7], Electro Fenton method [8] electro coagulation [9] electro chemical treatment [10] and so on. On the other hand, anilines which can be obtained by the catalytic hydrogenation of the aromatic nitrocompounds are vital intermediates in the field of agriculture, pharmaceuticals, dyes, polymers [11–13]. In recent years, chemical industries involve the production of aniline through the catalytic hydrogenation of nitrobenzene with precious metals like Pd, Pt, Au etc [14–16]. The high price and shortage of these precious metals limit their large-scale industrial applications. Moreover catalytic hydrogenation use low molecular weight, highly diffusible and inflammable hydrogen gas. In order to overcome these disadvantages, several reducing agents have been used for the reduction of nitroaromatics to the corresponding amines has widely been investigated over transition metal-based catalysts using reducing agents such as formic acid [17,18], hydrazine derivatives [19,20], sodium borohydride [21,22] and hydrosilanes [23]. Recently, bimetallic NPs have generated renewed interest in different fields like magnetic, optical and catalytic applications. Their catalytic activity and selectivity are clearly different from mono metallic counterparts [24–27]. Due to the combination of two metals, bimetallic NPs have additional degrees of freedom which give rise to synergism when used as catalysts [28]. Bimetallic heterogeneous catalysts, especially the non-precious, abundant, low cost and synthesized by relatively green methods are always in demanded for practical application [29]. In addition magnetically separable nanocatalysts are advantageous over traditional heterogeneous catalysts [30,31]. Moreover electron transfer of the catalyst system also enhances due to the presence of

magnetic phase (e.g., iron oxide) which can ultimately increase the efficiency of the catalyst.

In Chapter 6, we have discussed about the synthesis and characterization of Cu-Fe₂O₃ and CuNi NPs and their catalytic activity for the reduction of different nitroaromatic compounds.

This chapter is divided into two sections,

Section 6A: Facile Synthesis of Embedded Cu/Fe₂O₃ as Magnetically Recoverable Nanoparticles for Efficient Reduction of Nitroaromatics in Aqueous Medium at Room Temperature

Section 6B: Non-precious Magnetically Retrievable CuNi Alloy Catalyst: Transfer Hydrogenation of Nitroaromatics in 2-Propanol

Section 6A: Facile Synthesis of Embedded Cu/Fe₂O₃ as Magnetically Recoverable Nanoparticles for Efficient Reduction of Nitroaromatics in Aqueous Medium at Room Temperature

In this section of chapter 6 we have discussed about the synthesis of embedded Cu/Fe₂O₃ as magnetically recoverable NPs and characterized by different analytical techniques. The Cu/Fe₂O₃ NPs lead to mild and selective catalytic reductions of nitroaromatics in water at room temperature in presence of NaBH₄

6A.1. Results and Discussion

6A.1.1. Characterization of the Synthesized Cu/Fe₂O₃ NPs

The synthesized Cu/Fe₂O₃ NPs was thoroughly characterized by XRD, TEM, XPS and BET specific surface area. The crystal structure and purity of the NPs were first examined by XRD. As shown in Figure 6A.1a, the XRD pattern of Cu/Fe₂O₃ clearly establishes the formation of bimetallic fused cluster. The diffraction peaks at $2\theta = 43.4^\circ$, 50.9° and 74.0° can be indexed to (111), (200) and (220) crystal planes of fcc Cu [32] and peaks at $2\theta = 30.14^\circ$, 35.5° , 43.3° , 57° , and 62.5° corresponds to (220), (311), (400), (511), and (440) of γ -Fe₂O₃ (JCPDS no. 39-1346), respectively [33]. Moreover in the XRD pattern of Cu, the diffraction peaks at 43.5° , 50.8° and 74.2° could be index to (111), (200) and (220) crystal plans of fcc structure (JCPDS no. 85-1326). Likewise the diffraction peaks at $2\theta = 30^\circ$, 35.6° , 43.1° , 56.8° , and 62.4° corresponds to (220), (311), (400), (511), and (440) plans of cubic γ -Fe₂O₃. Figure 6A.1b represent the TGA analysis in air atmosphere from which dramatic mass gain of 12% between 150-365 °C was observed. This signifies the oxidation of metallic Cu in Cu/Fe₂O₃ in air atmosphere [34]. N₂ adsorption/desorption experiments was performed to investigate the surface and textural property of the synthesized NPs and presented in Figure 6A.1c. The BET surface area of Cu/Fe₂O₃ is calculated to be 30.3 m²/g.

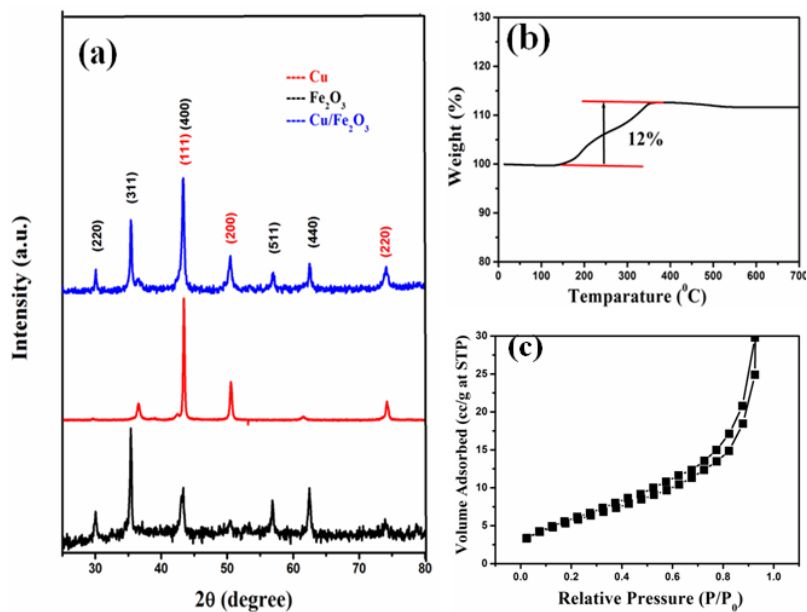


Figure 6A.1: (a) XRD patterns of the Fe₂O₃, Cu and Cu/Fe₂O₃, (b) TGA analysis of Cu/Fe₂O₃ in air atmosphere, and (c) N₂ adsorption-desorption isotherm of Cu/Fe₂O₃.

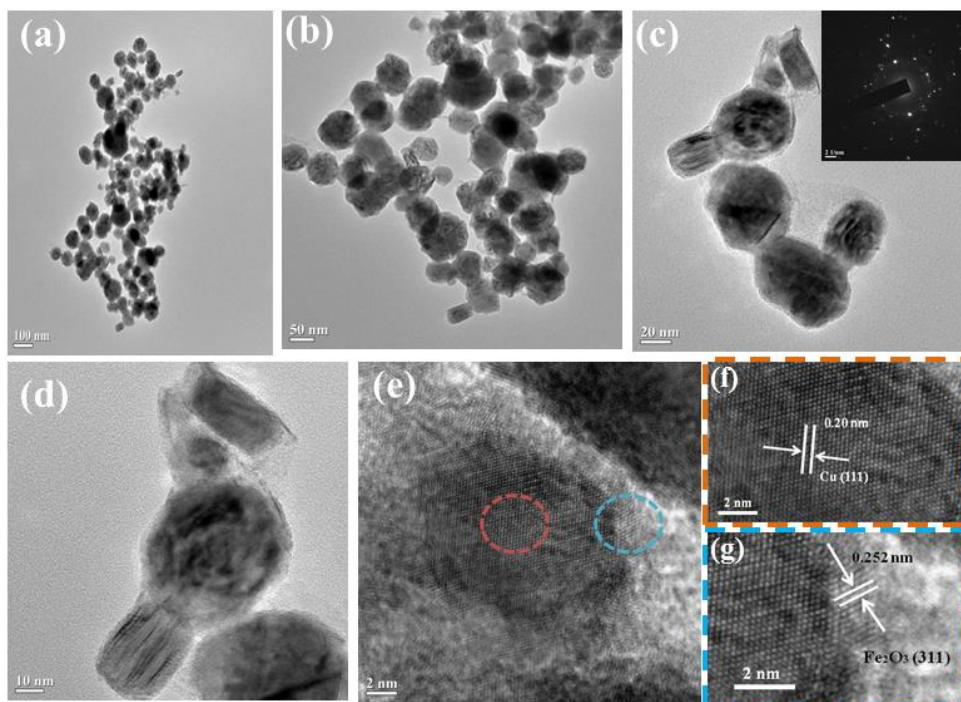


Figure 6A.2: (a-d) TEM images of Cu/Fe₂O₃, inset of (c) shows the SAED pattern and (e-g) HRTEM images of Cu/Fe₂O₃ showing the lattice fringes of Cu and Fe₂O₃.

TEM and HRTEM images of the Cu/Fe₂O₃ NPs are shown in Figure 6A.2. The particles crystallizes mostly in spherical shape in the size range of about 30–60 nm. Figure 6A.2(a-d). The micrographs indicated the nanostructure nature with some agglomeration, which is obvious because of the magnetic nature of the particles. HRTEM image of the marked region is shown in Figure 6A.2e and the crystal lattice fringes of Cu and Fe₂O₃ was clearly observed. The measured lattice spacing inside the NPs is 0.20 nm, corresponding to the (111) plane of Cu [35] (Figure 6A.2f) and 0.252 nm corresponding to the (311) plane of Fe₂O₃ [36] as shown in Figure 6A.2g. The SAED pattern Figure 6A.2g. The SAED pattern (inset of the Figure 6A.2c) shows bright spots forming ring structures, which are characteristics of polycrystalline nature of the NPs.

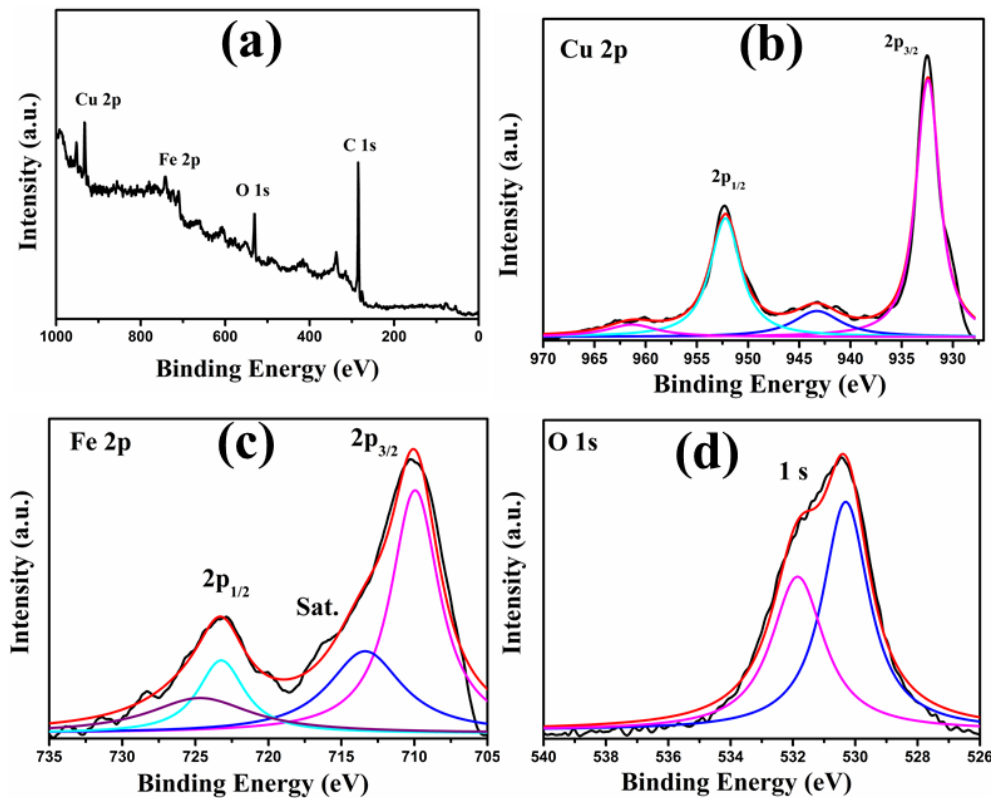


Figure 6A.3: (a) XPS survey spectrum of Cu/Fe₂O₃. High-resolution XPS spectra of (b) Cu 2p, (c) Fe 2p, and (d) O 1s for Cu/Fe₂O₃.

The Cu/Fe₂O₃ NPs are further analyzed by XPS, and the obtained results are shown in Figure 6A.3. The Figure 6A.3a represent the survey scan of the Cu/Fe₂O₃

NPs and all the peaks are indexed to Cu, Fe, O and C. The Cu 2p spectrum of the sample is shown in Figure 6A.3b. Two photoelectron peaks at binding energies of 932.2 and 952.3 eV can be observed which are assigned to Cu 2p_{3/2} and Cu 2p_{1/2} of zero-valent Cu, respectively [37]. Figure 6A.3c displays the Fe core-level XP spectrum of the NPs. Two peaks at 710 and 723.6 eV are clearly visible which correspond to the Fe 2p_{3/2} and Fe 2p_{1/2} core-level energies for iron oxide. Their positions are a clear indication that the iron oxide in our NPs is maghemite (γ -Fe₂O₃) [38–40]. The corresponding values for magnetite (Fe₃O₄) occur at slightly higher energies at 711.8 and 725.3 eV, respectively which evidence the absence of Fe₃O₄ [41]. Figure 6A.3d displays the XP spectra of O 1s level of the Cu/Fe₂O₃. The O 1s peak can be deconvoluted into two peaks at binding energies of 529.7 and 531.4 eV. The peak located at 529.7 eV is due to the lattice oxygen of the Fe₂O₃, and peak at 531.4 eV suggests some adsorbed species, such as, H₂O, OH, carbonate are present on the surface of the NPs [42].

6A.1.2 Catalytic Activity Studies monometallic Cu, Fe and Cu/Fe₂O₃ NPs

The catalytic reduction of 4-NP was carried out in the presence of monometallic Cu, Fe and Cu/Fe₂O₃ catalysts and aq. NaBH₄ as reducing agent. The 4-NP solution exhibits a strong absorption peak at ~315 nm in neutral or acidic conditions [43]. Upon addition of NaBH₄ solution, the absorption peak of 4-NP shifts from 315 to 400 nm immediately, which corresponds to a colour change of light yellow to yellow-green due to the formation of 4-nitrophenolate ion. After the addition of NPs, the colour of the 4-nitrophenolate ions diminishes after different time intervals for various NPs. Meanwhile, the characteristic absorption peak of 4-nitrophenolate ion at 400 nm gradually decreases, while a new peak at ~300 nm develops which is ascribed to 4-aminophenol (4-AP).

The catalytic data for the reduction of 4-NP to 4-AP over Cu/Fe₂O₃, Cu and Fe NPs are presented in Figure 6A.4. The metal NPs started the catalytic reduction by relaying electrons from the donor BH₄⁻ to the acceptor 4-NP right after the adsorption of both onto the particle surfaces. As the initial concentration of NaBH₄ was very high, it remained essentially constant throughout the reaction. For the evaluation of the

catalytic rate, the pseudo-first-order kinetics with respect to 4-NP is a reasonable assumption. (See chapter 2)

The K_{app} apparent rate constant of this catalytic reaction in the presence of different NPs are presented in Table 6A.1 as measured from the plot of $\ln(A_t/A_0)$ vs. time.

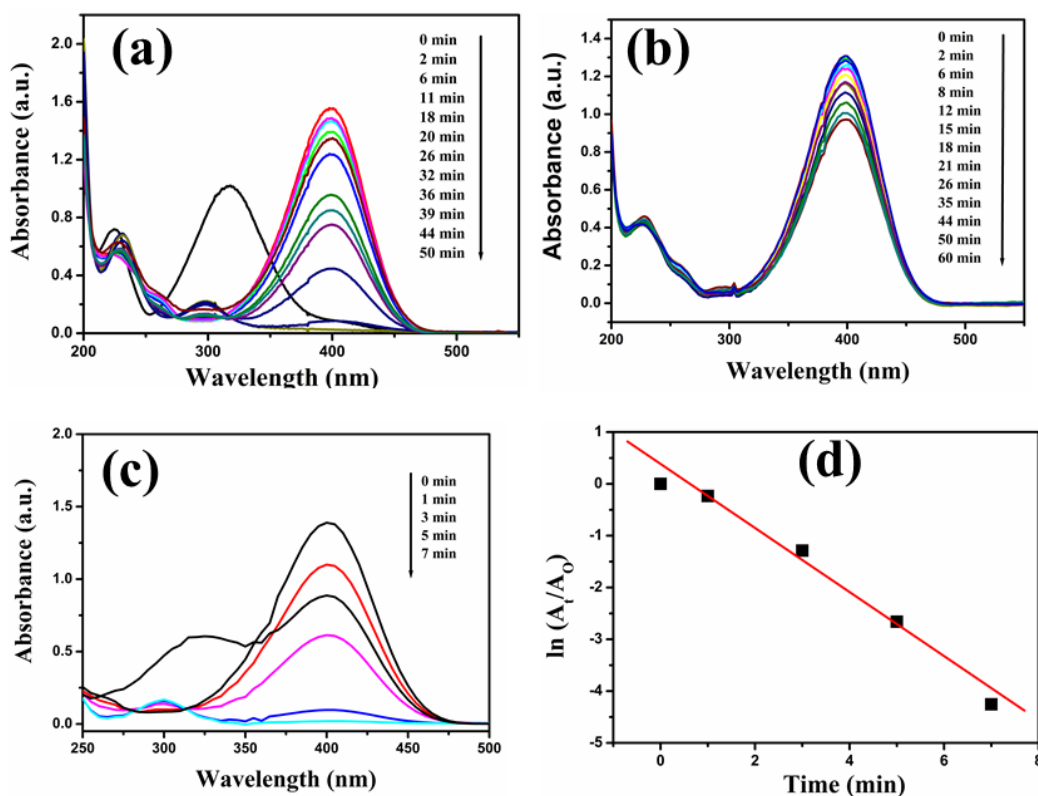


Figure 6A.4: Time-dependent absorption spectra of the reaction solution of 4-NP reduction to 4-AP over (a) Cu, (b) Fe_2O_3 , (c) Cu/ Fe_2O_3 and (d) plot of $\ln(A_t/A_0)$ against the reaction time of the catalytic reduction of 4-NP to 4-AP over Cu/ Fe_2O_3 .

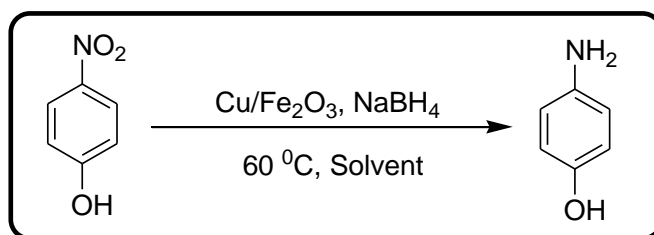
Table 6A.1: Comparison of k_{app} of Cu, Fe_2O_3 and Cu/ Fe_2O_3 for the reduction of 4-NP

SI No.	Catalyst	k_{app} ($\times 10^{-2} \text{ min}^{-1}$)
1	Cu/ Fe_2O_3	61.54
2	Cu	6.32
3	Fe	0.573

From these values it can be concluded that the Cu/Fe₂O₃ is superior in comparison to the other NPs for the reduction of 4-NP. This may be attributed to the unique physical and chemical properties possessed by Cu/Fe₂O₃ coupled due to synergistic effect of the both the metal.

6A.1.3: Catalytic Performance of the Cu/Fe₂O₃ NPs for the Reduction of Various Nitroaromatics

Table 6A.2: Optimization of Reaction Condition for the Reduction of 4-NP



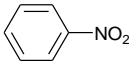
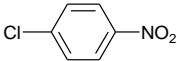
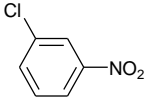
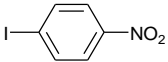
Entry	Catalyst (wt%)	NaBH ₄ (mmol)	Solvent (5 mL)	Time	Yield (%) ^b
1	10	5	MeOH	35 min	98
2	10	3	MeOH	35 min	96
3	5	3	MeOH	35 min	94
4	5	2	MeOH	35 min	78
5	5	3	EtOH	35 min	96
6	5	3	iPrOH	35 min	96
7	5	3	H ₂ O	45 min	92
8^c	5	3	H₂O	70 min	92
9	5	-	H ₂ O	400 min	20
10	-	3	H ₂ O	400 min	32

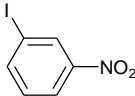

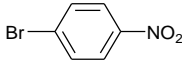
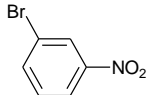
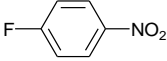

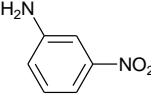
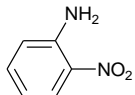

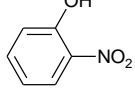
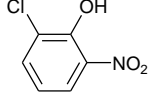
^aReaction condition: 1 mmol of 4-nitrophenol was used. ^bisolated yield, ^croom temperature

To examine the generality of the Cu/Fe₂O₃ catalytic system for the reduction of various nitrocompounds, at first, we carried out the reduction reaction in different condition to find out the optimized parameter of the reaction. When 10 wt% of

Cu/Fe₂O₃ catalyst and 5 mmol of NaBH₄ was used in the reduction of 4-NP (1 mmol) using MeOH at 60 °C, the reduction reaction results 98% yield in 60 min (Table 6A.2, entry 1). With decrease in the NaBH₄ amount to 3 mmol, the reaction results 96% yield in 60 min (Table 6A.2, entry 2). Further decrease of the catalyst amount to 5 mmol, a comparable yield of 94% (Table 6A.2, entry 3) was obtained. With 5 mmol catalysts and 3 mmol NaBH₄, optimizations were done in EtOH, iPrOH, and H₂O, in 60 °C (Table 6A.2, entries 5–7). To our delight, we observed that using H₂O, the reduction reaction proceeds with 92% isolated yield (Table 6A.2, entry 7). Therefore, the most suitable solvent for the reaction is H₂O. To further see the effect of temperature, we carried out experiment in room temperature obtained 92% yield. Therefore, further studies were conducted in room temperature using H₂O as solvent (Table 6A.2, entries 8). Moreover, when the reaction was performed without catalyst or NaBH₄ traces of the product could be found indicating that reduction proceeds only in the presence of metal catalyst and the reductant (Table 6A.2, entries 9–10). With the optimised reaction condition, a series of nitroaromatics with structurally diverse functional groups were examined. All the results are summarized in Table 6A.3. It could be seen that the reduction of all the functionalized nitroaromatics could be completed with high conversion and almost > 99% selectivity at room temperature and within a short time of less than 120 min.

Table 6A.3: Catalytic performances of the Cu/Fe₂O₃ NPs for reduction of various nitroaromatics using NaBH₄

Entry	Substrate	Reaction Time (min)	Conversion (%)	Selectivity (%)
1		80	>99	>99
2		40	>99	>99
3		50	>99	>99
4		50	>99	>99

5		60	>89.2	>99
6		60	>99	>99
7		50	>99	>99
8		60	>99	>99
9		60	>99	>99
10		70	>99	>99
11		80	>99	>99
12		90	>99	>99
13		70	>99	>99
14		60	>99	>99
15		100	>99	>99

^aReaction condition: 1 mmol of reactant, 5 wt% of catalyst, 3 mmol NaBH₄, room temperature, Conversion and Selectivity was analysed by GC-MS.

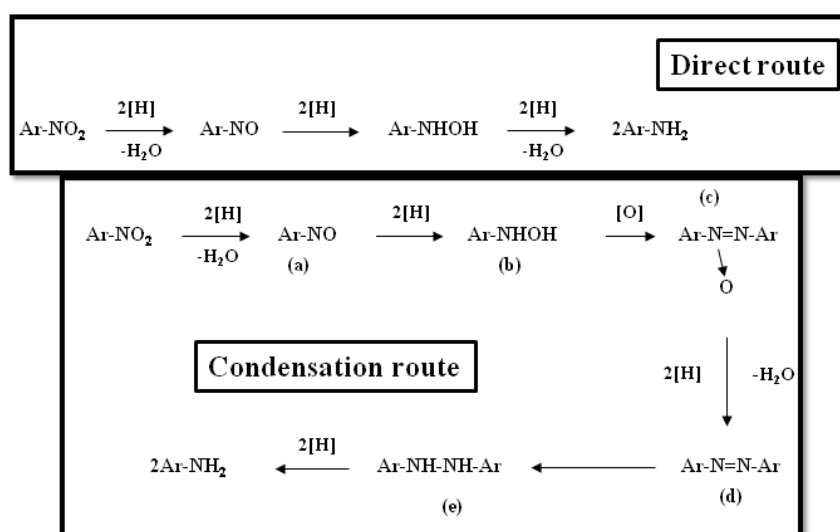
The halogen (F, Cl, Br, I)-substituted nitroaromatics selectively reduced to their corresponding anilines with no discernible dehalogenation (Table 6A.3 entries 2-5, 7-9). This is very important because, halogenated anilines are a series of vital intermediates and raw materials for the synthesis of drugs, pesticides, dyes, and photosensitive materials [44]. It was seen that *m*-substituted halonitroaromatic showed somewhat less reactivity compared to their *p*-substituted counterpart (Table 6A.3, entries 2 & 3, 4 & 5, 7 & 8). This concludes that our catalytic system is sensitive to steric effects. This type of similar observation was also observed by Fan and his co-

workers using ammonium formate and Au/TiO₂ as a catalyst [45]. The 4-NP takes less time to reduce the corresponding aniline than the 2-nitrophenol since the reaction proceeds through the formation of nitrophenolate ions (Table 6A.3, entries 13 and 14), [46,47]. 4-nitrophenolate ion is stable because the negative charge on the oxygen atom is effectively delocalised the benzene ring and the structure becomes resonance stabilized. 2-nitrophenolate is somewhat less stable than 4-nitrophenolate because of less effective resonance due to of steric effect. Other functional groups, such as amino 2-, 3-, 4-nitroaniline was also affording the corresponding aryl amines with high selectivities within 80 min (Table 6A.3, entry 12, 11, 10). Other electron donating group such p-toluidine also afforded excellent conversion and selectivity within 60 min. Moreover nitroaromatics with more than one substituted functional group also showed good conversion and selectivity to the respective anilines at little longer reaction times than the monosubstituted nitroaromatics. Table 6A.3, entry 15.

6A.1.4: Probable Reaction Mechanism for the Reduction of Nitroaromatics Catalyzed by the Cu/Fe₂O₃ NPs

According to the Layek et al. [48], the 4-NP with NaBH₄ reduction reaction usually proceeded in following ways. First, NaBH₄ ionises in aqueous medium with the production of BH₄⁻ which adsorb onto the surface of the metal NPs and react to form a metal hydride complex. Nitrocompounds also adsorbs onto the metal NPs surface and both of these processes are reversible i.e., adsorption accompanied by desorption. Once both the substrates are chemisorbed onto the metal NPs surface there is a hydrogen transfer from the metal hydride complex to the nitrocompounds. Based on the electrochemical model presented by Haber there are two probable routes for the reduction of nitro group to amino group, the direct route and the condensation route (see Scheme 6A.1) [48]. In the direct route, the aromatic nitrocompound is first reduced to the nitroso-compound and then further to the corresponding hydroxylamine in two very fast consecutive steps. Finally, the hydroxylamine is reduced to the aniline is the rate determining step of the reaction (direct route, see top in Scheme 6A.1). The second route involves the condensation of one molecule of the nitroso-compound with a molecule of the hydroxylamine to give the azoxy-compound, which sequentially gets reduced in a series of successive steps to the azo-, hydrazo-, and aniline-compounds

(condensation route, Scheme 6A.1). Layek et al. [48], Zhang et al. [49], Bendi et al. [50], and Liu et al. [51] proposed that NaBH_4 nitro reduction takes place by direct route, therefore it is reasonable to predict that the reduction process in this work undergoes via direct reduction route rather condensation route. Moreover, in the present case no azo- and azoxy-compounds are observed from UV-visible as well as GC-MS analyses. Thus the above results justify the direct route toward reduction of various nitroaromatics over $\text{Cu/Fe}_2\text{O}_3$ NPs.



Scheme 6A.1: Reaction mechanism proposed by Haber for reduction of nitroaromatics compounds.

6A.1.5: Reusability Studies of the $\text{Cu/Fe}_2\text{O}_3$ NPs and Kinetic Analysis

As a heterogeneous catalyst, one of the most significant factors is that it should be separated and reused easily. Herein, the recycle performance of the $\text{Cu/Fe}_2\text{O}_3$ is evaluated by 4-NP reduction monitored by UV-visible analyses of reaction solutions. In a typical procedure, to 20 mL (0.1 mmol L^{-1}) aqueous 4-NP purged with N_2 (to remove the dissolved oxygen) 5 mL (20 mmol L^{-1}) freshly prepared NaBH_4 was added. After the completion of the reaction, the contents were magnetically separated from the reaction mixture. The catalyst was then thoroughly washed with distilled water and used in the next cycle. This catalyst was used for another five reaction cycles. The conversion of 4-NP, k_{app} , and R^2 values were calculated following the procedures mentioned above and in chapter 2 and presented in Table 6A.4 and Figure

6A.5. It can be seen that there is a gradual decrease in k_{app} with each reaction cycle. Mainly it may be due to the gradual loss in weight of the catalyst during recycling or may be owing to changes in structure of the catalyst on repeated use.

Table 6A.4: Reusability Studies of the Cu/Fe₂O₃ NPs up to 5th cycles

Reaction Cycle	1 st	2 nd	3 rd	4 th	5 th
Conversion (%)	98	97	96	96	94
k_{app} ($\times 10^{-2} \text{ min}^{-1}$)	49.2	46.5	44.1	41.6	25.7
R^2	0.9953	0.98503	0.97922	0.99847	0.99454

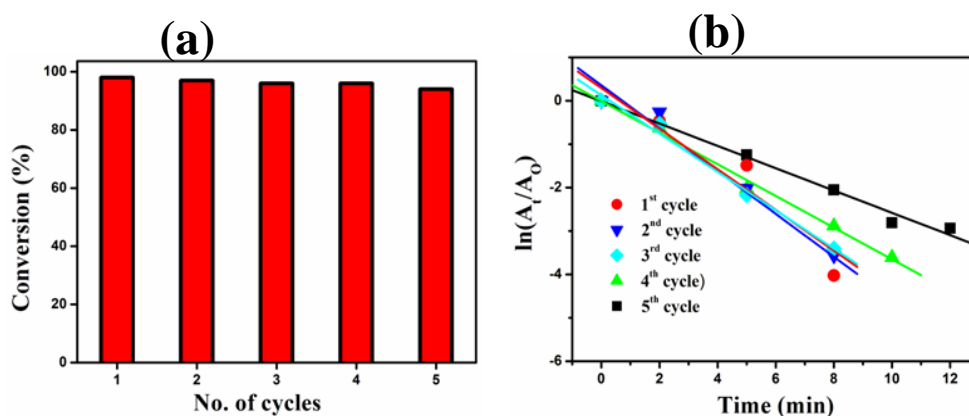


Figure 6A.5: (a) Conversion against number of cycles, (b) plot of $\ln(A_t/A_0)$ against the reaction time of the catalytic reduction of 4-NP to 4-AP for different cycles.

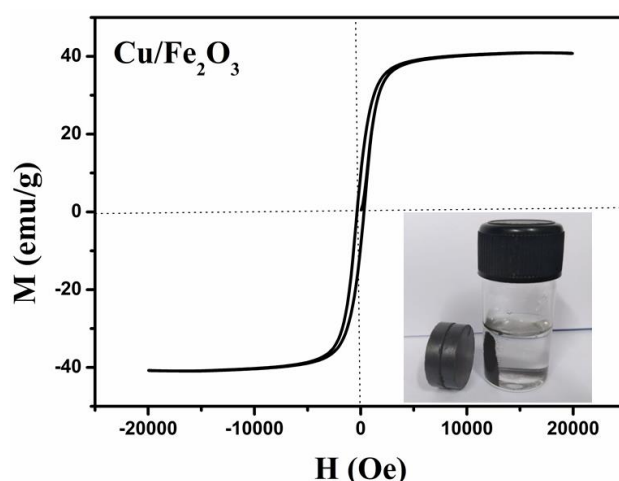


Figure 6A.6: The magnetic hysteresis loops of the Cu/Fe₂O₃ NPs. Inset shows the separation of Cu/Fe₂O₃ NPs from aqueous solution accomplished by an external magnet.

In order to confirm the magnetic properties of the hybrid Cu/Fe₂O₃ NPs VSM analysis was conducted at room temperature. The measurement shows that the Cu/Fe₂O₃ NPs have magnetization saturation value of 41.6 emu/g, as shown in Figure 6A.6. This data suggests that the NPs have superparamagnetism feature due to the nanosized maghemite, [52,53] which can be easily separated from their media by the use of an external magnetic field.

6A.2. Conclusions

In summary, we have reported the synthesis and characterization of embedded Cu/Fe₂O₃ NPs for the reduction of nitroaromatics in water at room temperature. The catalysts are highly capable and quantitatively reduce a variety of functionalized nitroaromatics to the corresponding aniline in >99% selectivity and conversion. It was seen that *m*-substituted halonitroaromatic showed somewhat less reactivity compared to their *p*-substituted counterpart. The halogen (F, Cl, Br)-substituted nitroaromatics are also reduced to their corresponding amines with no discernible dehalogenation. The catalyst is highly stable and can be reused up to 5th cycle without significant loss of catalytic activity.

Section 6B: Non-precious Magnetically Retrievable CuNi Alloy Catalyst: Transfer Hydrogenation of Nitroaromatics in 2-Propanol.

In the section, we demonstrate the synthesis and application of magnetically retrievable CuNi NPs for the reduction of nitroaromatics through transfer hydrogenation using 2-propanol. The CuNi NPs was prepared by hydrothermal method. The NPs exhibit unique catalytic activity for the reduction of various substituted nitroaromatics to the corresponding value-added products giving excellent yields of > 95%.

6B.1 Results and Discussion*6B.1.1 Characterization of the CuNi NPs*

The crystal structure and purity of CuNi NPs was examined by XRD and presented in Figure 6B.1. The characteristic peaks at $2\theta = 43.4^\circ$, 50.6° , and 74.4° corresponds to the crystal planes of (111), (200), and (220), respectively of fcc CuNi alloy (JCPDS 65-7246) with cell parameter, $a = 3.561 \text{ \AA}$. No impurity phases such as copper-nickel oxides and hydroxides were detected. Comparing the XRD pattern of the nanoalloy database of Cu (JCPDS 85-1326, $a = 3.615 \text{ \AA}$) and Ni (JCPDS 87-0712, $a = 3.523 \text{ \AA}$), it is clear that the diffraction peaks as well as unit cell parameter of the nanoalloy were located in between the corresponding peaks of Cu and Ni [54]. The nanoalloy patterns also show no evidence of any individual metallic peaks, which suggest that binary nucleation process has been the major nucleation process involved in the formation of these alloys [55].

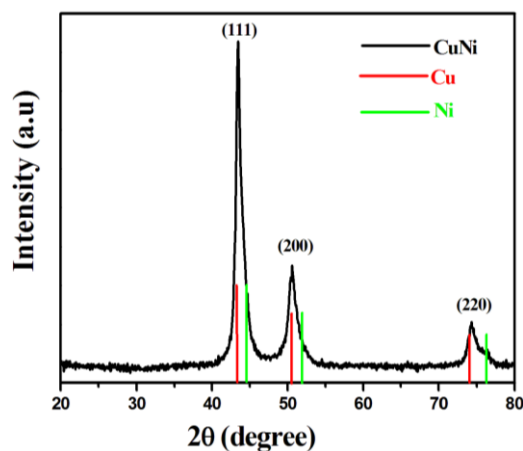


Figure 6B.1: XRD pattern of CuNi NPs along with diffraction lines from JCPDS database corresponding to Cu and Ni.

The morphology, size, and dispersion of the CuNi NPs were examined by TEM (Figure 6B.2a,b) and HR-TEM analyses (Figure 6B.2c,d). NPs showed a homogeneously distributed spherical shape and an average size of ~4-6 nm. HRTEM analysis shows the lattice fringe of ~0.19 nm which is characteristic of (111) facet on the CuNi NPs. Similar lattice fringes have also been observed for CuNi bimetallic NPs [56]. The SAED pattern of the NPs shows in the inset of the Figure 6B.2d which clearly exhibit bright spots forming rings confirming the polycrystalline nature of the NPs.

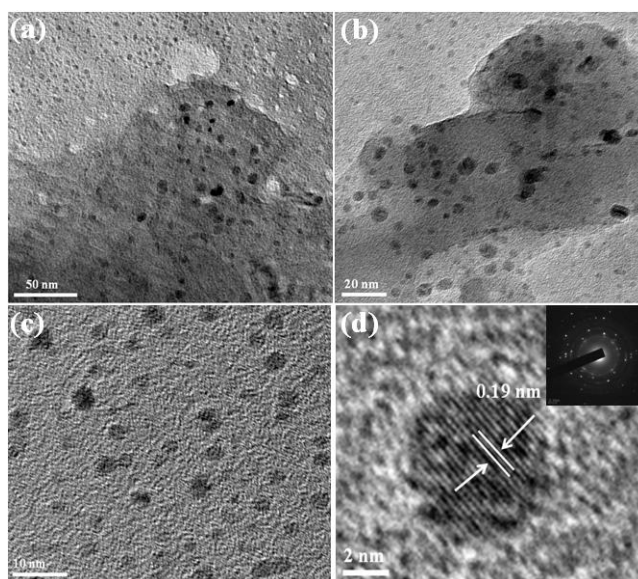


Figure 6B.2: TEM (a,b) and HR-TEM (c,d) of CuNi NPs. Inset in the figure (d) shows the SAED pattern of the NPs.

XPS is commonly employed to characterize the surface chemical states and composition of NPs. The presence of strong XPS signals at ~853 and ~931.7 eV in the survey spectrum of CuNi NPs corresponds to Ni 2p and Cu 2p respectively (Figure 6B.3a). For the Cu 2p spectrum (Figure 6B.3b), the photoelectron peaks at binding energies of 932.16 and 952.05 eV corresponds to the Cu 2p_{3/2} and Cu 2p_{1/2} of Cu. From the deconvoluted spectra it has been observed that the binding energies of 934.08 and 954.10 eV is also present, which corresponds to the Cu 2p_{3/2} and Cu 2p_{1/2} of Cu²⁺ states respectively [57]. Moreover, two additional peaks at binding energies of 943.17 and 962.87 eV are also noticed, which are assigned to shake-up satellite of Cu

$2p_{3/2}$ and Cu $2p_{1/2}$, respectively [58,59]. This specifies the existence of CuO on the surface. The existence of other valence states on the surface were due to the high oxophilicity of Cu(0), which has high affinity to form oxides under aerobic atmosphere. The Ni 2p XP spectrum of CuNi NPs is shown in Figure 6B.3c. Two peaks at binding energies of 854.4 and 870.8 eV can be observed, which are assigned to Ni $2p_{3/2}$ and Ni $2p_{1/2}$ of zero-valent Ni, respectively [60]. Moreover, the peaks at 854.4 and 873.2 eV are index to the Ni²⁺ $2p_{3/2}$ and Ni²⁺ $2p_{1/2}$ state, Additionally, the appearance of two strong satellite peaks, are observed corresponding to Ni $2p_{3/2}$ (859.6 eV) and $2p_{1/2}$ (878.4 eV) [61,62]. The O 1s photoelectron can be deconvoluted into two peaks at binding energies of 530.3 and 531.9 eV. The peak located at 530.3 eV is due to the lattice oxygen of the CuNi NPs, and other peak at 531.9 eV corresponds to the NPs adsorbed oxygen species on the surface [63]. (Figure 6B.3d)

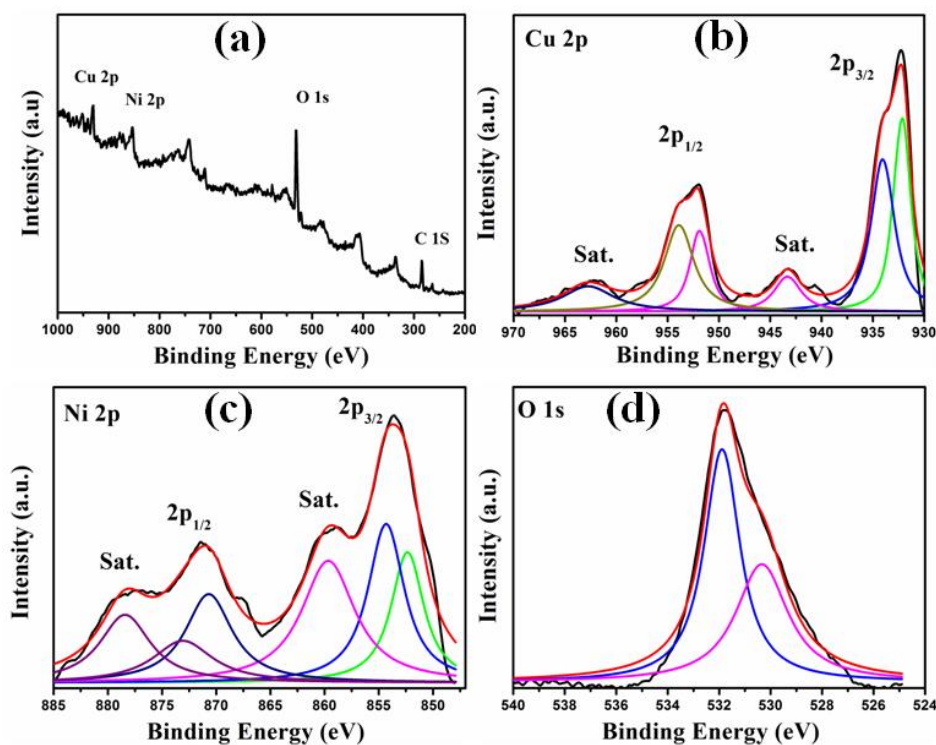
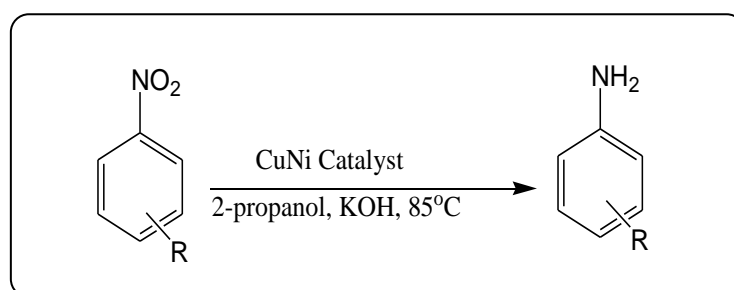


Figure 6B.3: (a) XPS survey spectra of CuNi, core level XP spectra of (b) Cu 2p and (c) Ni 2p and (d) O1s.

6B.1.2 Catalytic performance of the CuNi NPs

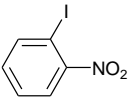
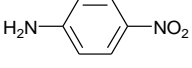
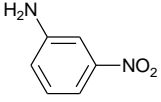
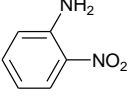
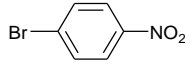
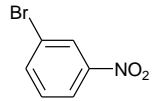

1 mmol of the reactant was dissolved in 10 mL 2-propanol followed by addition of 15 wt% of catalyst and 3 mmol KOH to a two neck 100 mL round bottom flask. The reaction mixture was refluxed at 83 °C for the required time period. The progress of the reaction was monitored by TLC. After the completion of the reaction, the catalyst was separated from the reaction mixture by centrifugation. The catalyst was first washed with distilled water and then with acetone to eliminate any traces of organic substance. The filtrate containing the reaction mixture was extracted with HPLC grade ethyl acetate and dried over anhydrous Na_2SO_4 , the conversion/selectivity and product identification were done by GC-MS analysis.



Scheme 6B.1: Transfer hydrogenation of nitroaromatics to corresponding anilines over bimetallic CuNi NPs.

Table 6B.1: Catalytic performances of the CuNi NPs for reduction of various nitroaromatics using 2-propanol KOH as base

Entry	Substrate	Reaction time (h)	Conversion (%)	Products Selectivity		
				Aniline (%)	Azo (%)	Azoxy (%)
1.		7	98	56	10	34
2.		8	100	82	12	6
3.		8.5	100	75	20	5
4.		4	100	94	4	2
5.		4.5	100	67.5	26.5	6

6.		5	100	70	22	8
7.		9	100	86	10	4
8.		6	100	82	12	6
9.		8	100	80	12	8
10.		5	100	75	18	7
11.		5.5	90.7	97.5	2.5	-
12.		6	100	93	5	2

Reaction Conditions: 1 mmol of nitroaromatics, 15 wt% of catalyst, 3 mmol KOH and 10 mL of 2-propanol refluxed at 85 °C. Selectivity/Conversion was determined by GC-MS.

To examine the scope of the CuNi catalytic system for the catalytic transfer hydrogenation of the nitro-group, a series of nitroaromatics with structurally diverse functional groups were examined. The catalytic system was found to be very efficient regardless of the presence of electron-donating or electron-withdrawing substituents in the aromatic ring as conversion of the reaction was more than 90% (Entry 4 and 12 Table 6B.1). Reduction data shows that along with corresponding aniline other intermediate products like azo- and azoxy-compounds are also formed. Although the azo- and azoxy-products are formed as side product, these compounds have great value in the field of medicine, dye, polymer etc. Moreover, in case of halonitroaromatics, current catalyst system can efficiently convert to halogenated anilines without unwanted dehalogenated product (Entry 1-6, 10, 11). For heterogeneous catalyst, recyclability is the crucial matter for the practical application of the catalyst, recyclability tests of the catalyst were carried out using 4-iodo-1-nitrobenzene, reused the recovered catalyst up to three times (Table 6B.2). The catalyst was collected with

an external magnet. The catalyst was first washed with distilled water (3 x 15 mL) to remove the excess base and then with acetone (3 x 15 mL) to eliminate any traces of organic substance. The catalyst was vacuum dried at 55 °C before using in the next run. The reactions were carried out by keeping the stoichiometry of reactant and recovered catalyst as earlier. Results show that the catalyst remains active up to three cycles without significant lost in catalytic activity. The recovered catalyst was further characterized by XRD (Figure 6B.4a). The recovered catalyst showed some oxide phase of CuO, as the catalyst exposed to air during catalytic study.

Table 6B.2. Recyclability test of the reduction of 4-iodo 1-nitrobenzene with CuNi catalyst system

No. of runs	Isolated yield
1	92
2	90
3	88

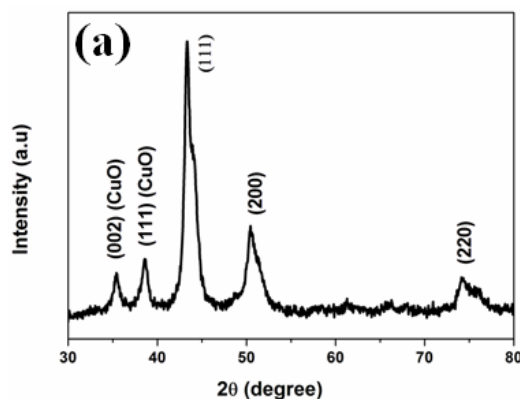


Figure 6B.4: (a) XRD pattern of CuNi NPs after three catalytic cycles.

6B.1.3: Plausible Reaction Mechanism for the Reduction of Nitroaromatics Catalyzed by the CuNi NPs through Transfer Hydrogenation

Based on the electrochemical model as presented by Haber there are two possible routes for the reduction of nitro group to amino group, the direct route and the condensation route. (Scheme 6A.1) [64]. Subramanian et al. have beautifully demonstrated that the direct route is the preferred pathway for the transfer hydrogenation of nitrocompounds on Cu-NPs/zeolite when reaction was carried out in

autoclave bomb and condensation route is preferred pathway when reaction was carried out in oil bath [65]. In the present case to obtain an insight into the reaction pathway involved in CuNi catalyzed reduction, the presence of azoxy- and azo-benzene in the reaction mixture probably signifies that the condensation route is the preferred one for reduction. Thus it may be concluded that the condensation route involving nitrobenzene \rightarrow nitrosobenzene \rightarrow phenylhydroxylamine \rightarrow azoxy \rightarrow azo \rightarrow hydrazo \rightarrow aniline is the most likely path followed for the catalytic transfer hydrogenation of nitroaromatics using CuNi NPs and 2-propanol act as both solvent and reducing agent. To confirm whether the reduction of nitroaromatics catalyzed by CuNi NPs follows a heterogeneous pathway, we tried to scrutinize the reaction by two different method (i) filtration test and (ii) Hg-poisoning test. At first we started two reactions in two separate RB by taking 4-iodobenzene as substrate and maintaining the reaction condition as described in the experimental section. After 2 h when the reactant converted nearly 50%, from first RB the catalyst was separated from the reaction mixture and allowed the reaction to continue. In 2nd RB access mercury was added to the reaction mixture and the reaction was continued. After continuing the reaction for 5 h no conversion was observed in both the RB. This observation suggests that the reaction follows the heterogeneous pathway.

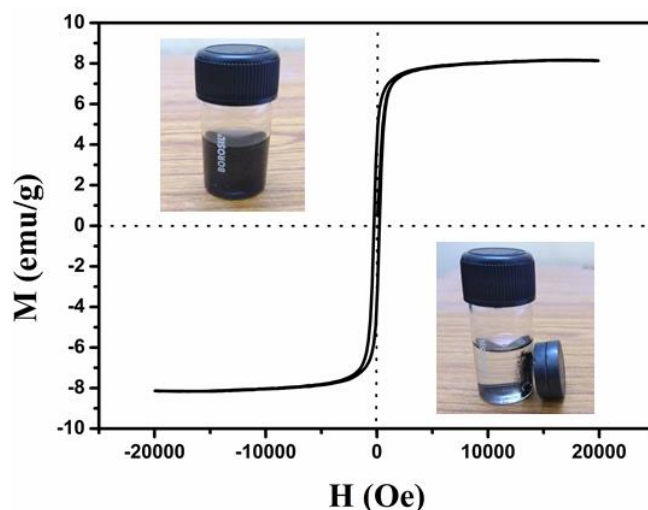


Figure 6B.5: Room-temperature magnetization curve of the CuNi NPs.

Table 6B.3: Comparison table for previously reported catalytic system for the reduction of nitrobenzene through transfer hydrogenation:

Entry.	Catalytic system	H ₂ Source	Solvent/Base	Temperature (°C) / Time (h)	Yield (%)	Ref.
1	Pd(OAc) ₂	PSF	DMF/ -	120/ 6-12	<90	68
2	Au NPs	2-propanol	-/ KOH	40/6	100	76
3	Ni-MCM-41	2-propanol	-/ KOH	Reflux/ 3.5- 5	>75	78
4	Cu-NPs/zeolite	2-propanol	-/-	80/ 1-3	>90	65
5	Ru ⁰ -AT-Mont	2-propanol	-/ NaOH	82/ 4-12	>98	75
6	Fe ₃ O ₄ /C	2-propanol	-/ KOH	85/ 0.6-0.3	>99	69
7	Ru(II)/ligand	2-propanol	-/ NaO ⁱ Pr	110/5	>98	70
8	[RuCl ₂ (PPh ₃) ₂]	HCOOH	EtOH/ Et ₃ N	125/5	>90	71
9	ReIO ₂ (PPh ₃) ₂	PhMe ₂ SiH	Toluene/ -	Reflux/ 1-45	>98	72
10	Cu NPs	HCOONH ₄	Ethylene glycol/ -	120/ 12	>90	73
11	FeBr ₂ PPh	PhSiH ₃	Toluene/ -	110/ 16	<99	74
12	Ag-Fe ₃ O ₄ -GD GD=Graphene derivative	2-propanol	-/ KOH	100/24	96	77

Figure 6B.5 shows the magnetic properties of the CuNi NPs at room temperature. CuNi NPs exhibited a saturation magnetization of approximately 8.17 emu/g which corresponds to super paramagnetic properties; this magnetic property value is essential to recover the catalyst from the reaction mixture with an external magnet for reuse [66,67]. The inset of Figure 6B.5 shows the magnetic separation of CuNi NPs which can be easily recovered from the reaction mixture using an external magnet avoiding complex separation. The outstanding magnetic property makes the NPs system as easily reusable catalyst. Finally, a glimpse of our quick survey on the reduction of nitroaromatic compound through transfer hydrogenation over different catalysts is presented in Table 6B.3.

6B.2. Conclusions

In summary, we present an efficient and practical approach for the synthesis of various value-added compounds from corresponding nitroaromatics using CuNi alloy NPs whose catalytic activity is comparable to those of precious metals. This is ascribed to the remarkable synergistic effect between Cu and Ni as confirmed by XRD and XPS analyses. Moreover by careful examination of the NPs through XPS analysis, it is found that the successful combination metallic CuNi with oxide CuO-NiO. This can induce the whole CuNi/CuO-NiO NPs. The presence of both the metallic and oxide phase in the NPs, the electroflipping between various oxidation states of the Cu and Ni is easier, which can ultimately promote the catalytic activity by enhancing the electron transport during the reduction of a variety of nitroaromatics. Additionally, the catalyst can be easily separated by filtration as well as by an external magnet. The use of 2-propanol as both solvent and reducing agent instead of other harmful and risky reducing agent makes the process very efficient. Moreover, the replacement of precious metal catalysts with less-expensive transition metal in many transformation reactions will be of great significance due to the less availability and high cost of noble metals.

References

- [1] Borah, B. J., and Bharali, P. Surfactant-free synthesis of CuNi nanocrystals and their application for catalytic reduction of 4-nitrophenol. *Journal of Molecular Catalysis A: Chemical*, 390:29–36, 2014.
- [2] Mulchandani, P., Hangarter, C. M., Lei, Y., Chen, W., and Mulchandani, A. Amperometric microbial biosensor for p-nitrophenol using *Moraxella* sp.-modified carbon paste electrode. *Biosensors and Bioelectronics*, 21(3):523–527, 2005.
- [3] Niaz, A., Fischer, J., Barek, J., Yosypchuk, B., Sirajuddin, and Bhangar, M. I. Voltammetric determination of 4-nitrophenol using a novel type of silver amalgam paste electrode. *Electroanalysis*, 21(16):1786–1791, 2009.
- [4] Lipczynska-Kochany, E. Degradation of aqueous nitrophenols and nitrobenzene by means of the Fenton reaction. *Chemosphere*, 22(5-6):529–536, 1991.

- [5] Marais, E., and Nyokong, T. Adsorption of 4-nitrophenol onto Amberlite IRA-900 modified with metallophthalocyanines. *Journal of Hazardous Materials*, 152(1):293–301, 2008.
- [6] O'Connor, O. A., and Young, L. Y. Toxicity and anaerobic biodegradability of substituted phenols under methanogenic conditions. *Environmental Toxicology and Chemistry*, 8(10):853–862, 1989.
- [7] Dieckmann, M. S., and Gray, K. A. A comparison of the degradation of 4-nitrophenol via direct and sensitized photocatalysis in TiO₂ slurries. *Water Research*, 30(5):1169–1183, 1996.
- [8] Oturan, M. A., Peiroten, J., Chartrin, P., and Acher, A. J. Complete destruction of p-nitrophenol in aqueous medium by electro-Fenton method. *Environmental Science & Technology*, 34(16):3474–3479, 2000.
- [9] Modirshahla, N., Behnajady, M. A., and Mohammadi-Aghdam, S. Investigation of the effect of different electrodes and their connections on the removal efficiency of 4-nitrophenol from aqueous solution by electrocoagulation. *Journal of Hazardous Materials*, 154(1-3):778–786, 2008.
- [10] Canizares, P., Saez, C., Lobato, J., and Rodrigo, M. A. Electrochemical treatment of 4-nitrophenol-containing aqueous wastes using boron-doped diamond anodes. *Industrial & engineering chemistry research*, 43(9):1944 – 1951, 2004.
- [11] Kleist, W., Pröckl, S. S., Drees, M., Köhler, K., and Djakovitch, L. Amination of aryl chlorides and fluorides toward the synthesis of aromatic amines by palladium-catalyzed route or transition metal free way: Scopes and limitations. *Journal of Molecular Catalysis A: Chemical*, 303(1–2):15-22, 2009.
- [12] Deka, P., Borah, B. J., Saikia, H., and Bharali, P. Cu-based nanoparticles as emerging environmental catalysts. *The Chemical Record*, 19(2-3):462 – 473, 2019.
- [13] Saikia, H., Borah, B. J., and Bharali, P. Room temperature reduction of nitroaromatics using pd nanoparticles stabilized on Nano-CeO₂. *Chemistry Select*, 2(32):10524–10530, 2017.
- [14] Du, Y., Chen, H., Chen, R., and Xu, N. Synthesis of p-aminophenol from p-nitrophenol over nano-sized nickel catalysts. *Applied Catalysis A: General*,

- 277(1-2):259–264, 2004.
- [15] Saikia, H., Borah, B. J., Yamada, Y., and Bharali, P. Enhanced catalytic activity of CuPd alloy nanoparticles towards reduction of nitroaromatics and hexavalent chromium. *Journal of Colloid and Interface Science*, 486:46–57, 2017.
- [16] Vaidya, M. J., Kulkarni, S. M., and Chaudhari, R. V. Synthesis of p-aminophenol by catalytic hydrogenation of p-nitrophenol. *Organic process research & development*, 7(2):202–208, 2003.
- [17] Jagadeesh, R. V., Banerjee, D., Arockiam, P. B., Junge, H., Junge, K., Pohl, M.-M., Radnik, J., Brückner, A., and Beller, M. Highly selective transfer hydrogenation of functionalised nitroarenes using cobalt-based nanocatalysts. *Green Chemistry*, 17(2): 898–902, 2015.
- [18] Datta, K. J., Rathi, A. K., Gawande, M. B., Ranc, V., Zoppellaro, G., Varma, R. S., and Zboril, R. Base-free transfer hydrogenation of nitroarenes catalyzed by micro-mesoporous iron oxide. *ChemCatChem*, 8(14):2351–2355, 2016.
- [19] Cantillo, D., Baghbanzadeh, M., and Kappe, C. O. In situ generated iron oxide nanocrystals as efficient and selective catalysts for the reduction of nitroarenes using a continuous flow method. *Angewandte Chemie International Edition*, 51(40):10190–10193, 2012.
- [20] Jiang, C., Shang, Z., and Liang, X. Chemoselective transfer hydrogenation of nitroarenes catalyzed by highly dispersed, supported nickel nanoparticles. *ACS Catalysis*, 5(8):4814–4818, 2015.
- [21] Wang, C., Ciganda, R., Salmon, L., Gregurec, D., Irigoyen, J., Moya, S., Ruiz, J., and Astruc, D. Highly efficient transition metal nanoparticle catalysts in aqueous solutions. *Angewandte Chemie International Edition*, 55(9):3091 – 3095, 2016.
- [22] Yang, F., Chi, C., Wang, C., Wang, Y., and Li, Y. High graphite N content in nitrogen-doped graphene as an efficient metal-free catalyst for reduction of nitroarenes in water. *Green Chemistry*, 18(15):4254–4262, 2016.
- [23] Fountoulaki, S., Daikopoulou, V., Gkizis, P. L., Tamiolakis, I., Armatas, G. S., and Lykakis, I. N. Mechanistic studies of the reduction of nitroarenes by NaBH₄ or hydrosilanes catalyzed by supported gold nanoparticles. *ACS Catalysis*, 4(10):3504–3511, 2014.

- [24] Burda, C., Chen, X., Narayanan, R., and El-Sayed, M. A. Chemistry and properties of nanocrystals of different shapes. *Chemical reviews*, 105(4):1025–1102, 2005.
- [25] Ferrando, R., Jellinek, J., and Johnston, R. L. Nanoalloys: from theory to applications of alloy clusters and nanoparticles. *Chemical reviews*, 108(3):845–910, 2008.
- [26] Rodriguez, J. A., and Goodman, D. W. The nature of the metal-metal bond in bimetallic surfaces. *Science*, 257(5072):897–903, 1992.
- [27] Tao, F., Grass, M. E., Zhang, Y., Butcher, D. R., Renzas, J. R., Liu, Z., Chung, J. Y., Mun, B. S., Salmeron, M., and Somorjai, G. A. Reaction-driven restructuring of Rh-Pd and Pt-Pd core-shell nanoparticles. *Science*, 322(5903):932–934, 2008.
- [28] Tokonami, S., Morita, N., Takasaki, K., and Toshima, N. Novel synthesis, structure, and oxidation catalysis of Ag/Au bimetallic nanoparticles. *The Journal of Physical Chemistry C*, 114(23):10336–10341, 2010.
- [29] Borah, B. J., Saikia, H., and Bharali, P. Reductive conversion of Cr (VI) to Cr (III) over bimetallic CuNi nanocrystals at room temperature. *New Journal of Chemistry*, 38(7):2748–2751, 2014.
- [30] Das, V. K., Mazhar, S., Gregor, L., Stein, B. D., Morgan, D. G., Maciulis, N. A., Pink, M., Losovyj, Y., and Bronstein, L. M. Graphene derivative in magnetically recoverable catalyst determines catalytic properties in transfer hydrogenation of nitroarenes to anilines with 2-propanol. *ACS Applied Materials & Interfaces*, 10(25):21356–21364, 2018.
- [31] Rossi, L. M., Silva, F. P., Vono, L. L. R., Kiyohara, P. K., Duarte, E. L., Itri, R., Landers, R., and Machado, G. Superparamagnetic nanoparticle-supported palladium: a highly stable magnetically recoverable and reusable catalyst for hydrogenation reactions. *Green Chemistry*, 9(4):379–385, 2007.
- [33] Liu, R., Liu, J.-F., Zhang, L.-Q., Sun, J.-F., and Jiang, G.-B. Low temperature synthesized ultrathin γ -Fe₂O₃ nanosheets show similar adsorption behaviour for As(III) and As(V). *Journal of Materials Chemistry A*, 4(20):7606–7614, 2016.
- [34] Wu, D., Wen, M., Lin, X., Wu, Q., Gu, C., and Chen, H. A NiCo/NiO–CoO_x ultrathin layered catalyst with strong basic sites for high-performance H₂

- generation from hydrous hydrazine. *Journal of Materials Chemistry A*, 4(17):6595–6602, 2016.
- [35] Liang, Y., Chen, Z., Yao, W., Wang, P., Yu, S., and Wang, X. decorating of Ag and CuO on Cu nanoparticles for enhanced high catalytic activity to the degradation of organic pollutants. *Langmuir*, 33(31):7606–7614, 2017.
- [36] Cao, D., Li, H., Pan, L., Li, J., Wang, X., Jing, P., Cheng, X., Wang, W., Wang, J., and Liu, Q. High saturation magnetization of γ -Fe₂O₃ nano-particles by a facile one-step synthesis approach. *Scientific Reports*, 6(1):32360, 2016.
- [37] Li, H., Guo, C.-Y., and Xu, C.-L. A highly sensitive non-enzymatic glucose sensor based on bimetallic Cu–Ag superstructures. *Biosensors and Bioelectronics*, 63:339–346, 2015.
- [38] Gole, A., Stone, J. W., Gemmill, W. R., zur Loye, H.-C., and Murphy, C. J. Iron oxide coated gold nanorods: synthesis, characterization, and magnetic manipulation. *Langmuir*, 24(12):6232–6237, 2008.
- [39] Sun, Y., Duan, L., Guo, Z., DuanMu, Y., Ma, M., Xu, L., Zhang, Y., and Gu, N. An improved way to prepare superparamagnetic magnetite-silica core-shell nanoparticles for possible biological application. *Journal of Magnetism and Magnetic Materials*, 285(1-2):65–70, 2005.
- [40] Teng, X., Black, D., Watkins, N. J., Gao, Y., and Yang, H. Platinum-maghemite core-shell nanoparticles using a sequential synthesis. *Nano Letters*, 3(2):261–264, 2003.
- [41] Kokate, M., Dapurkar, S., Garadkar, K., and Gole, A. Magnetite–silica–gold nanocomposite: one-pot single-step synthesis and its application for solvent-free oxidation of benzyl alcohol. *The Journal of Physical Chemistry C*, 119(25):14214–14223, 2015.
- [42] Han, Q., Liu, Z., Xu, Y., Chen, Z., Wang, T., and Zhang, H. Growth and properties of single-crystalline γ -Fe₂O₃ nanowires. *The Journal of Physical Chemistry C*, 111(13):5034–5038, 2007.
- [43] Deka, P., Deka, R. C., and Bharali, P. In situ generated copper nanoparticle catalyzed reduction of 4-nitrophenol. *New Journal of Chemistry*, 38(4):1789–1793, 2014.
- [44] Cárdenas-Lizana, F., Gómez-Quero, S., and Keane, M. A. exclusive production

- of chloroaniline from chloronitrobenzene over Au/TiO₂ and Au/Al₂O₃. *ChemSusChem*, 1(3):215–221, 2008.
- [45] Lou, X.-B., He, L., Qian, Y., Liu, Y.-M., Cao, Y., and Fan, K.-N. Highly chemo- and regioselective transfer reduction of aromatic nitro compounds using ammonium formate catalyzed by supported gold nanoparticles. *Advanced Synthesis & Catalysis*, 353(2-3):281–286, 2011.
- [46] Praharaj, S., Nath, S., Ghosh, S. K., Kundu, S., and Pal, T. Immobilization and recovery of Au nanoparticles from anion exchange resin: resin-bound nanoparticle matrix as a catalyst for the reduction of 4-nitrophenol. *Langmuir*, 20(23):9889–9892, 2004.
- [47] Lee, J., Park, J. C., and Song, H. A nanoreactor framework of a Au@SiO₂ yolk/shell structure for catalytic reduction of p-Nitrophenol. *Advanced Materials*, 20(8):1523–1528, 2008.
- [48] Haber, F. Z. Gradual electrolytic reduction of nitrobenzene with limited cathode potential. *Elektrochem. Angew. Phys. Chem.*, 22:506–514, 1898
- [49] Zhang, P., Shao, C., Zhang, Z., Zhang, M., Mu, J., Guo, Z., and Liu, Y. In situ assembly of well-dispersed Ag nanoparticles (AgNPs) on electrospun carbon nanofibers (CNFs) for catalytic reduction of 4-nitrophenol. *Nanoscale*, 3(8):3357, 2011.
- [50] Bendi, R., and Imae, T. Renewable catalyst with Cu nanoparticles embedded into cellulose nano-fiber film. *RSC Advances*, 3(37):16279–16282, 2013.
- [51] Liu, W.-J., Tian, K., Jiang, H., and Yu, H.-Q. Harvest of Cu NP anchored magnetic carbon materials from Fe/Cu preloaded biomass: their pyrolysis, characterization, and catalytic activity on aqueous reduction of 4-nitrophenol. *Green Chemistry*, 16(9):4198–4205, 2014.
- [52] Larsen, G. K., Farr, W., and Hunyadi Murph, S. E. Multifunctional Fe₂O₃–Au nanoparticles with different shapes: enhanced catalysis, photothermal effects, and magnetic recyclability. *The Journal of Physical Chemistry C*, 120(28):15162–15172, 2016.
- [53] Sun, Z., Yue, Q., Liu, Y., Wei, J., Li, B., Kaliaguine, S., Deng, Y., Wu, Z., and Zhao, D. Rational synthesis of superparamagnetic core–shell structured mesoporous microspheres with large pore sizes. *Journal of Materials Chemistry*

- A, 2(43):18322–18328, 2014.
- [54] Boone, C. V., and Maia, G. Pt–Pd and Pt–Pd–(Cu or Fe or Co)/graphene nanoribbon nanocomposites as efficient catalysts toward the oxygen reduction reaction. *Electrochimica Acta*, 247:19–29, 2017.
- [55] Muñoz-Flores, B. M., Kharisov, B. I., Jiménez-Pérez, V. M., Elizondo Martínez, P., and López, S. T. Recent advances in the synthesis and main applications of metallic nanoalloys. *Industrial & Engineering Chemistry Research*, 50(13):7705–7721, 2011.
- [56] Zhang, Y., Huang, W., Habas, S. E., Kuhn, J. N., Grass, M. E., Yamada, Y., Yang, P., and Somorjai, G. A. Near-monodisperse Ni–Cu bimetallic nanocrystals of variable composition: controlled synthesis and catalytic activity for H₂ generation. *The Journal of Physical Chemistry C*, 112(32):12092–12095, 2008.
- [57] Fang, H., Wen, M., Chen, H., Wu, Q., and Li, W. Graphene stabilized ultra-small CuNi nanocomposite with high activity and recyclability toward catalysing the reduction of aromatic nitro-compounds. *Nanoscale*, 8(1):536–542, 2016.
- [58] Dubale, A. A., Pan, C.-J., Tamirat, A. G., Chen, H.-M., Su, W.-N., Chen, C.-H., Rick, J., Ayele, D. W., Aragaw, B. A., Lee, J.-F., Yang, Y.-W., and Hwang, B.-J. Heterostructured Cu₂O/CuO decorated with nickel as a highly efficient photocathode for photoelectrochemical water reduction. *Journal of Materials Chemistry A*, 3(23):12482–12499, 2015.
- [59] Yen, H., Seo, Y., Kaliaguine, S., and Kleitz, F. Role of metal–support interactions, particle size, and metal–metal synergy in CuNi nanocatalysts for H₂ generation. *ACS Catalysis*, 5(9):5505–5511, 2015.
- [60] Bhattacharjee, D., and Dasgupta, S. Trimetallic NiFePd nanoalloy catalysed hydrogen generation from alkaline hydrous hydrazine and sodium borohydride at room temperature. *Journal of Materials Chemistry A*, 3(48):24371–24378, 2015.
- [61] Li, W., Zhao, Z., Guo, X., and Wang, G. Employing a nickel-containing supramolecular framework as Ni precursor for synthesizing robust supported Ni catalysts for dry reforming of methane. *ChemCatChem*, 8(18):2939–2952, 2016.

- [62] She, W., Qi, T., Cui, M., Yan, P., Ng, S. W., Li, W., and Li, G. High catalytic performance of a CeO₂-supported Ni catalyst for hydrogenation of nitroarenes, fabricated via coordination-assisted strategy. *ACS Applied Materials & Interfaces*, 10(17):14698–14707, 2018.
- [63] Huang, J., Han, J., Wang, R., Zhang, Y., Wang, X., Zhang, X., Zhang, Z., Zhang, Y., Song, B and Jin, S. Improving electrocatalysts for oxygen evolution using Ni_xFe_{3-x}O₄/Ni hybrid nanostructures formed by solvothermal synthesis. *ACS Energy Letters*, 3(7):1698–1707, 2018.
- [64] Layek, K., Kantam, M. L., Shirai, M., Nishio-Hamane, D., Sasaki, T., and Maheswaran, H. Gold nanoparticles stabilized on nanocrystalline magnesium oxide as an active catalyst for reduction of nitroarenes in aqueous medium at room temperature. *Green Chemistry*, 14(11):3164–3174, 2012.
- [65] Subramanian, T., and Pitchumani, K. Selective reduction of nitroarenes by using zeolite-supported copper nanoparticles with 2-propanol as a sustainable reducing agent. *ChemCatChem*, 4(12):1917–1921, 2012.
- [66] Xiong, R., Wang, Y., Zhang, X., Lu, C., and Lan, L. In situ growth of gold nanoparticles on magnetic γ -Fe₂O₃@cellulose nanocomposites: a highly active and recyclable catalyst for reduction of 4-nitrophenol. *RSC Advances*, 4(13):6454–6462, 2014.
- [67] Larsen, G. K., Farr, W., and Hunyadi Murph, S. E. Multifunctional Fe₂O₃–Au nanoparticles with different shapes: enhanced catalysis, photothermal effects, and magnetic recyclability. *The Journal of Physical Chemistry C*, 120(28):15162–15172, 2016.
- [68] Basu, B., Das, P., and Das, S. Transfer hydrogenation using recyclable polymer-supported formate (PSF): Efficient and chemoselective reduction of nitroarenes. *Molecular Diversity*, 9(4):259–262, 2005.
- [69] Veerakumar, P., Panneer Muthuselvam, I., Hung, C.-T., Lin, K.-C., Chou, F.-C., and Liu, S.-B. Biomass-derived activated carbon supported Fe₃O₄ nanoparticles as recyclable catalysts for reduction of nitroarenes. *ACS Sustainable Chemistry & Engineering*, 4(12):6772–6782, 2016.
- [70] Paul, B., Chakrabarti, K., Shee, S., Maji, M., Mishra, A., and Kundu, S. A simple and efficient in situ generated ruthenium catalyst for chemoselective

- transfer hydrogenation of nitroarenes: kinetic and mechanistic studies and comparison with iridium systems. *RSC Advances*, 6(102):100532 – 100545, 2016.
- [71] Watanabe, Y., Ohta, T., Tsuji, Y., Hiyoshi, T., and Tsuji, Y. Ruthenium catalyzed reduction of nitroarenes and azaaromatic compounds using formic acid. *Bulletin of the Chemical Society of Japan*, 57(9):2440–2444, 1984.
- [72] de Noronha, R. G., Romão, C. C., and Fernandes, A. C. Highly chemo- and regioselective reduction of aromatic nitro compounds using the system silane/oxo-rhenium complexes. *The Journal of Organic Chemistry*, 74(18):6960–6964, 2009.
- [73] Saha, A., and Ranu, B. Highly chemoselective reduction of aromatic nitro compounds by copper nanoparticles/ammonium formate. *The Journal of Organic Chemistry*, 73(17):6867–6870, 2008.
- [74] Junge, K., Wendt, B., Shaikh, N., and Beller, M. Iron-catalyzed selective reduction of nitroarenes to anilines using organosilanes. *Chemical Communications*, 46(10):1769–1771, 2010.
- [75] Sarmah, P. P., and Dutta, D. K. Chemoselective reduction of a nitro group through transfer hydrogenation catalysed by Ru⁰-nanoparticles stabilized on modified Montmorillonite clay. *Green Chemistry*, 14(4):1086–1093, 2012.
- [76] Zhu, H., Ke, X., Yang, X., Sarina, S., and Liu, H. Reduction of nitroaromatic compounds on supported gold nanoparticles by visible and ultraviolet light. *Angewandte Chemie International Edition*, 49(50):9657–9661, 2010.
- [77] Das, V. K., Mazhar, S., Gregor, L., Stein, B. D., Morgan, D. G., Maciulis, N. A., Pink, M., Losovyj, Y., and Bronstein, L. M. Graphene derivative in magnetically recoverable catalyst determines catalytic properties in transfer hydrogenation of nitroarenes to anilines with 2-propanol. *ACS Applied Materials & Interfaces*, 10(25):21356–21364, 2018.
- [78] Mohapatra, S. K., Sonavane, S. U., Jayaram, R. V., and Selvam, P. Regio- and chemoselective catalytic transfer hydrogenation of aromatic nitro and carbonyl as well as reductive cleavage of azo compounds over novel mesoporous NiMCM-41 molecular sieves. *Organic letters*, 4(24):4297–4300, 2002.